Available online at www.sciencedirect.com
SCIENCE DIRECT®
International Journal of Thermal Sciences 42 (2003) 523–532
International Journal of Thermal Sciences
www.elsevier.com/locate/ijts

A new indicator for knock detection in gas SI engines

Guillaume Brecq, Jérôme Bellettre *, Mohand Tazerout

Département systèmes énergétiques et environnement, Ecole des mines de Nantes, La Chantrerie, 4, rue Alfred Kastler, B.P. 20722, 44307 Nantes cedex 3, France

Received 25 June 2001; accepted 8 July 2002

Abstract

Determination of knock onset for any engine tuning remains a difficult work for many engine manufacturers. This study investigates different combinations of existing knock indices in order to produce an upgraded indicator, which is easier to calibrate. Experiments are conducted on a single-cylinder gas engine bounded to combined heat and power (CHP). Effects of spark advance, volumetric efficiency and equivalent ratio are studied under constant speed operation. The ratio $IMPO/(MAPO \times W)$ (with *IMPO* defined as the Integral of Modulus of Pressure Oscillations, *MAPO* as the Maximum Amplitude of Pressure Oscillations and W as the width of the computational window) is proposed as suitable indice. In any engine setting, it remains constant under no knocking conditions. When knock occurs, a model deduced from dimensionless analysis allows determination of the oversteps of Knock Limited Spark Advance from a single $IMPO/(MAPO \times W)$ measurement with an accuracy better than 1 CA. Knock is then studied for different gas qualities by adding propane or carbon dioxide to the fuel. The results show that there is no significant effect of the fuel composition on the proposed indicator, making the model able to calculate *KLSA* overstep in all the situations.

Keywords: SI engine; Knock; Indicator; Pressure signal; High frequency; Natural gas; Propane concentration; Carbon dioxide concentration

1. Introduction

The economical and environmental concerns incite engine manufacturers to set higher and higher compression ratio. Over the past sixty years, the mean operational compression ratio increased from 5 : 1 to 12 : 1 for spark ignition engines. High compression ratio engines are particularly sensitive to knock, that-is-to-say uncontrolled auto-ignition that, if persistent, can lead to severe damages and even to the engine destruction.

This paper focuses on gas engines often used in combined heat and power (CHP) operation or that can be used in other fields such as automotive applications. These have to face to a variable fuel quality, in terms of anti-knock properties, since they mainly use network natural gas, whose the composition can change with location and time. Consequently, among Spark Ignition (SI) engines, gas engines are fundamentally more prone to knock. In order to maintain a constant knock margin (defined as the difference between current spark advance and that corresponding to knock onset), it is particularly important to be able to detect precisely, reliably and on line when knock occurs.

Knock indices are normally obtained from data generated by either accelerometers or cylinder pressure sensors. Due to its simplicity, accelerometry (vibration measurement) is largely employed in industry. Nevertheless, parasitic noise related to engine operation often affect the quality of knock detection in this method. On the other hand, cylinder pressure data provide a direct and reliable way to analyse knock. The major disadvantage is the relatively high cost of the probes directly fixed in the cylinder head of the engine. However, recent developments in indirect in-cylinder pressure measurements support the idea that cylinder pressure will no longer be costly to acquire, even in industrial engines [1,2]. These could be equipped with production instrumentation capable of assessing the combustion process on line. Therefore, a knock detection method based on cylinder pressure analysis could be soon applied to numerous industrial cases.

Several studies have been carried out to develop suitable indices [3,4] and to compare them [5–8]. Most knock indices are extracted from the in-cylinder pressure signal because of their direct connection with knock phenomenon.

* Corresponding author.
E-mail address: jerome.bellettre@emn.fr (J. Bellettre).

1290-0729/02/$ – see front matter
doi:10.1016/S1290-0729(02)00052-2

Nomenclature

DKI	Dimensionless Knock Indicator
IMPO	Integral of Modulus of Pressure Oscillations ..... bar·CA
KLSA	Knock Limited Spark Advance ..... CA
MAPO	Maximum Amplitude of Pressure Oscillations ..... bar
$\tilde{p}$	filtered pressure ..... bar
NL	Noise Level of $IMPO/(MAPO \times W)$
SA	Spark Advance BTDC (Before Top Dead Centre) ..... CA
ST	Spark Timing ..... CA
W	width of computational window ..... CA

Greek symbols

ϕ	equivalence ratio
η_v	volumetric efficiency

Superscript

$^\circ$	without the "noise" of the deflagration

One of the most frequently used indices is likely the maximum amplitude of the pressure oscillations (*MAPO*). This indicator is defined later in the paper.

The aim of this paper is to propose a general knock indicator applied to SI engines. Experiments are performed on a gas engine under a large range of operating conditions including study of the effect of the gas composition. Two different existing indices are combined in order to enhance the properties of the knock detection tools.

2. Experimental setup

2.1. Test bench

Experiments are conducted on a naturally aspirated single-cylinder SI gas operated engine of Lister–Petter make. Its main technical features are presented in Table 1. The engine is connected to an electrical generator, which maintained the speed at 1500 rev·min^{-1} (to generate 50 Hz electrical power). Engine and main measurements are presented in Fig. 1.

The engine is based on a DI Diesel engine, with bowl chamber and flat-faced cylinder head. It is adapted to SI operation by reducing its compression ratio and by fixing a spark plug in the injector hole. The carburation system and the gas discharge unit are shown in Fig. 2.

The data acquisition system of the pressure within the cylinder and in the inlet manifold is composed of:

– Sensor AVL QH32D, gain 25.28 pC·bar^{-1}—range 0–200 bar;

Table 1
Engine technical features

Maximal power	6 kW
Maximal Torque	38.2 N·m
Bore	95.3 mm
Stroke	88.9 mm
Displacement	633 cm^3
Compression ratio	12.4 : 1
Cooling system	Forced air circulation

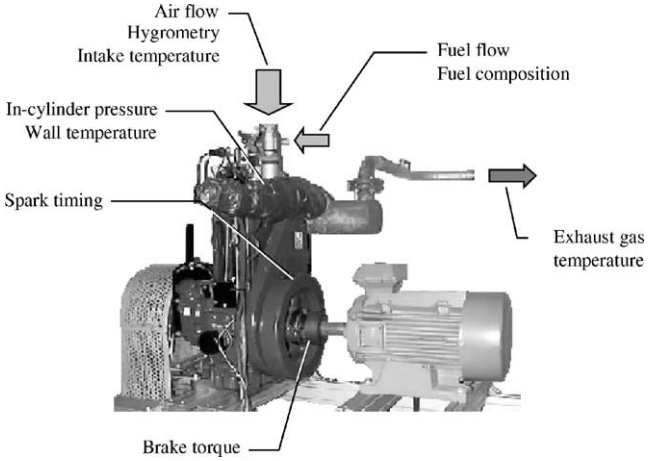

Fig. 1. Test rig and main sensor locations.

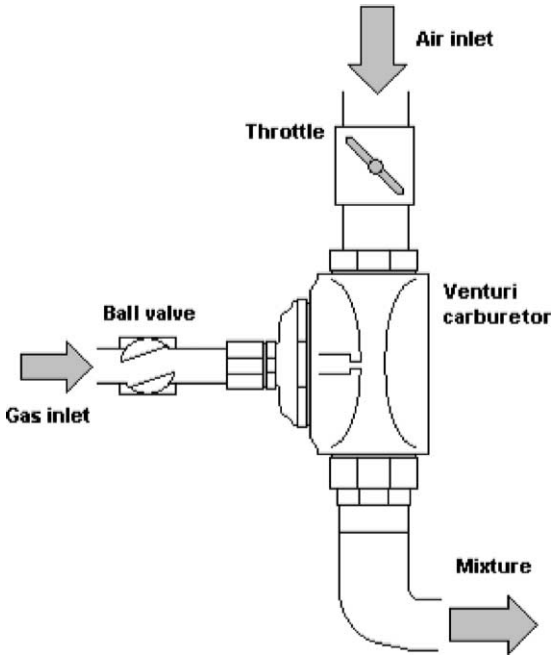

Fig. 2. Carburation system and gas discharge unit.

– Piezo amplifier AVL 3066A0, gain 400 pC·V^{-1} with no pressure reference;
– Piezo resistive pressure sensor fixed inside the inlet manifold—range 0–2.5 bar.

The acquisition frequency is 90 kHz (i.e., a resolution of 0.1 CA degree).

Natural gas used is analysed by a gas chromatograph. The mean composition of the natural gas is given in Table 2 with its maximum fluctuations. Exhaust gases are analysed by a COSMA Cristal 500 analyser. The measurement of the O_2 and CO_2 concentration allows the calculation of the equivalence ratio ϕ (with an inaccuracy lower than 4% compared to the ratio of inlet flows).

2.2. Experimental method

The engine is run at a constant speed (1500 rev·min^{-1}) and at different levels of fuel air ratio and volumetric efficiency. The spark advance is varied from spark advances slightly below MBT (maximum brake torque) setting (i.e., 5–15 degree BTDC—Before Top Dead Centre), to values corresponding to heavy knock (15–45 degree BTDC depending on tuning). During each experiment, the throttle position is kept constant.

On the one hand, only low values of equivalence ratio match with normal CHP operation. On the other hand, automotive engines mainly run with $\phi \approx 1$. It is then decided to analyse four different levels of ϕ (0.70, 0.80, 0.90 and 1.00) between these two kinds of operation. ϕ is maintained constant during each experiment by controlling the exhaust gas composition.

The volumetric efficiency η_v is fixed at three constant values: 73, 77 and 82%. It is controlled by measuring continuously both air and fuel mass flow.

An increase in the spark advance tends to make the combustion start earlier and shifts the peak pressure towards the TDC. This raises the pressure and the temperature of end gas and leads to auto-ignition. Thus, the range of experiments covers no knock to high knocking conditions. The engine is stabilised before measurements.

Table 2
Mean natural gas composition

	Volumetric content	Max. absolute fluctuation
CH_4	90.4%	±1.7%
C_2H_6	6.7%	±1.6%
C_3H_8	1.8%	±0.8%
C_xH_y	0.7%	±0.5%
N_2	0.3%	±0.3%

2.3. Signal pressure analysis

Cylinder pressure signals are analysed by an on line system to compute knock indices. The indices used in the study are based on the high frequency analysis of cylinder pressure data. The first indicator is called integral of modulus of pressure oscillations (*IMPO*). It is a way to represent the energy contained in the high frequency oscillations of the cylinder pressure signal, which occurs due to knock. The second one is called maximum amplitude of pressure oscillations (*MAPO*). It is related to the peak of the pressure oscillations, which occurs due to knock. Thus, both these parameters use pressure oscillations resulting from knock as the input. Many authors use them to define the intensity of the knock generated in the cylinder.

After being processed in a band-pass filter (4–20 kHz), the pressure signal is rectified and processed to give *MAPO* and *IMPO*, as illustrated in Fig. 3. *IMPO* and *MAPO* are obtained for each cycle. They are calculated on a 60-degree Crank Angle window starting with the spark timing. In this study, the average value of *IMPO* and *MAPO* are obtained from 400 consecutive cycles (except where otherwise stated).

IMPO and *MAPO* can be expressed as:

$$IMPO = \frac{1}{N}\sum_{1}^{N}\int_{ST}^{ST+W} |\tilde{p}|\,\mathrm{d}\theta \tag{1}$$

$$MAPO = \frac{1}{N}\sum_{1}^{N}\max_{ST,ST+W} |\tilde{p}| \tag{2}$$

where N represents the number of computed cycles, ST the spark timing in crank angle degrees, $\tilde{p}$ the filtered pressure and W the width of the computational window (here 60 CA).

In the present work, the *IMPO* and *MAPO* online computation is done by the "Indiwin" software developed by AVL Society.

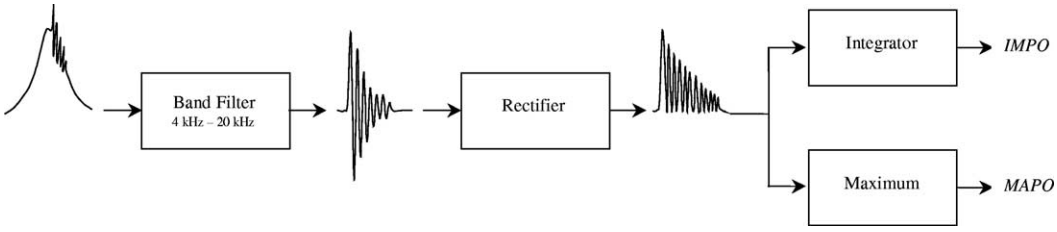

Fig. 3. Sketch of knock indices determination.

3. Use of existing knock indices

3.1. Experimental results

Experimental data are acquired under variable spark advances and constant equivalence ratios (ϕ) and volumetric efficiencies (η_v). *MAPO* and *IMPO* are measured with uncertainties summarised in Table 3. The error on spark advance adjustment is estimated at ± 0.2 CA.

Knock is generated by increasing progressively the spark advance starting from MBT setting to consistent knock. Effects of the three different levels of volumetric efficiency and four equivalence ratios on *MAPO* and *IMPO* are indicated in Figs. 4 and 5. Finally, we define the knock limited spark advance (*KLSA*) as the highest spark advance reachable without knock.

Table 3
Experimental uncertainties

	Without knock	With knock
IMPO	±1%	±4%
MAPO	±3%	±7%

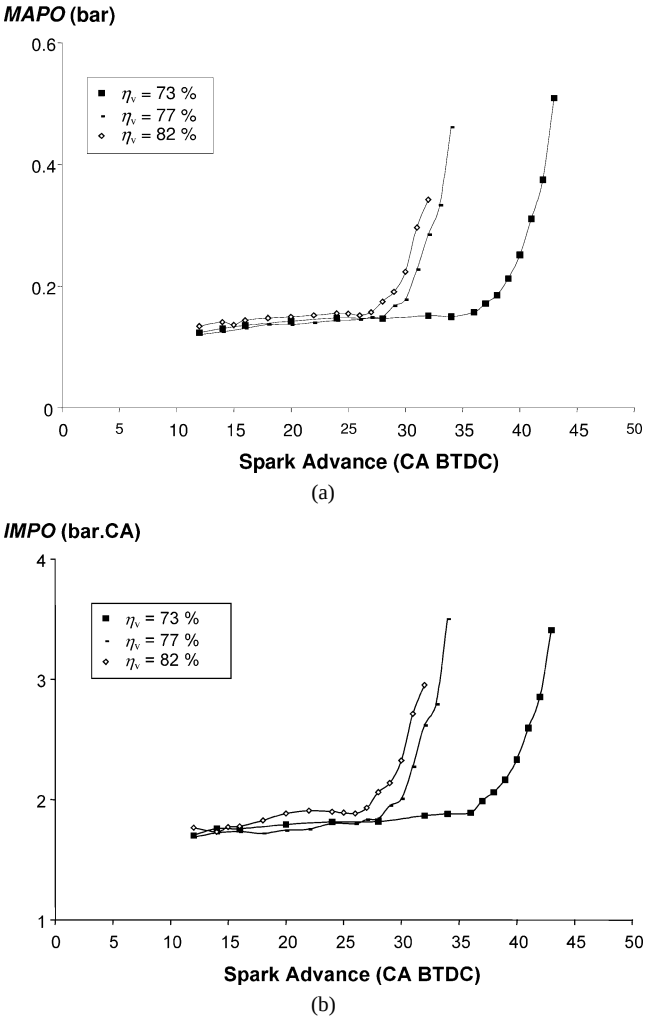

Fig. 4. (a) Effect of volumetric efficiency on *MAPO* ($\phi = 0.7$); (b) Effect of volumetric efficiency on *IMPO* ($\phi = 0.7$).

3.2. Difficulties in KLSA determination

Two methods to determine *KLSA* are mainly reported in literature:

(1) The first method is based on the sudden increase of *MAPO* or *IMPO*. It is established by Najt [9] who uses *MAPO* versus spark advance for different fuels to determine *KLSA*. It requires many measurements both in normal and in knocking conditions.
(2) The second method determines when *IMPO* or *MAPO* exceed a certain threshold level. Most authors [5,10–12] use this latter method, because it is easy to employ once the threshold is fixed and can be computed on line. This second method is used in the present work, because it is the only one that can be applied in industry.

From Figs. 4 and 5, it is obvious that *KLSA* tends to lower spark advance when both fuel air ratio and volumetric

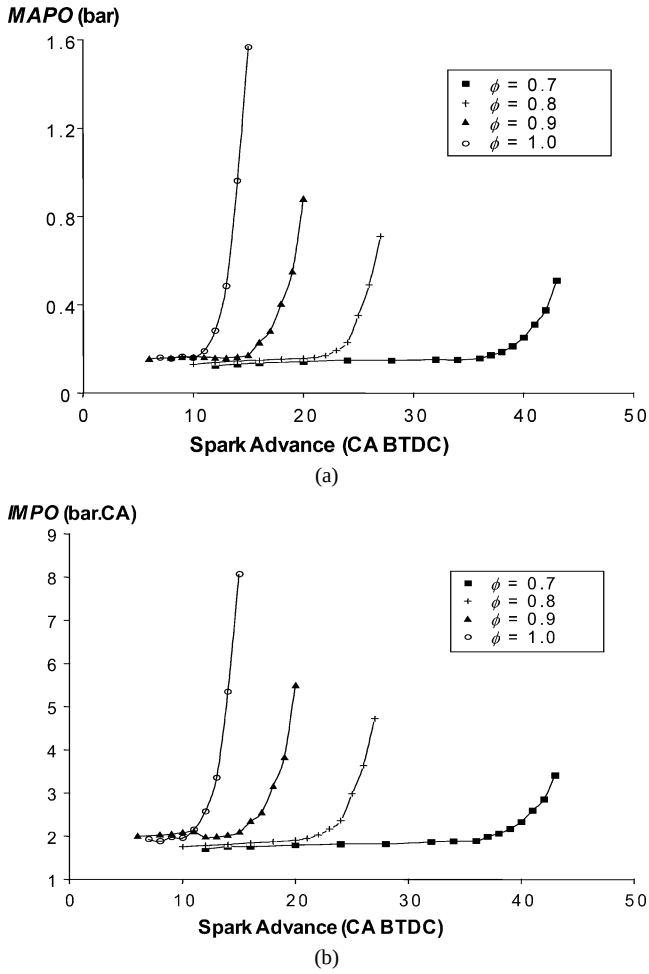

Fig. 5. (a) Effect of equivalence ratio on *MAPO* ($\eta_v = 73\%$); (b) Effect of equivalence ratio on *IMPO* ($\eta_v = 73\%$).

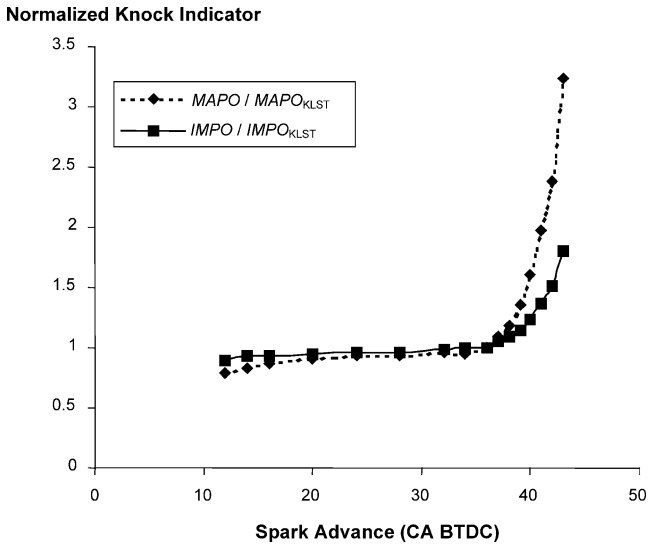

Fig. 6. Comparison between standard knock indices versus spark advance ($\phi = 0.7$ and $\eta_v = 73\%$).

efficiency are increased. Diana et al. [7] compared *MAPO* and *IMPO* with variable compression ratio and fuel quality. No significant difference could be observed: both indices provided identical results. The effect of the spark advance is shown in Fig. 6 deduced from Figs. 4 and 5. Same trends can be observed. This confirms Diana et al. observations. Consequently, both *IMPO* and *MAPO* can be used to determine the start of knock.

The choice of an indicator is still a matter of disagreement for numerous authors since no ideal indicator has been yet established [5]. Hence, even if similar trends can be noticed on Figs. 4 and 5, the application of method (2) does not give a unique threshold level beyond which it can be assumed that knock occurs. The threshold level closely depends on engine features. Thomas et al. [11] use a *MAPO* threshold level at 90 kPa whereas Goto and Itoh [12] define their no knock level at 7 kPa. Moreover, it also depends on the frequency of the band-pass filter employed. Puzinauskas [5] determines two different levels of *MAPO* (15 kPa or 23 kPa) depending of the band pass filter used (4–9 kHz or 4–12 kHz). Figs. 3 and 4 indicate that the threshold level depends on the engine operating conditions. Thus, the determination of a threshold level is a long work and leads Millo and Ferraro [6] to conclude that the knock threshold should be not only adapted to engine but also to operating conditions and its selection should be based on a solid statistical analysis. For these reasons, such indicators as *IMPO* or *MAPO* used separately can only provide a rough determination of knock threshold level and is always submitted to difficult calibration.

4. Dimensionless indicator for knock detection

Dimensionless analysis could be helpful to develop a general knock indicator independent of engine setting. Assuming that spark advance, *SA*, equivalence ratio, ϕ, volumetric

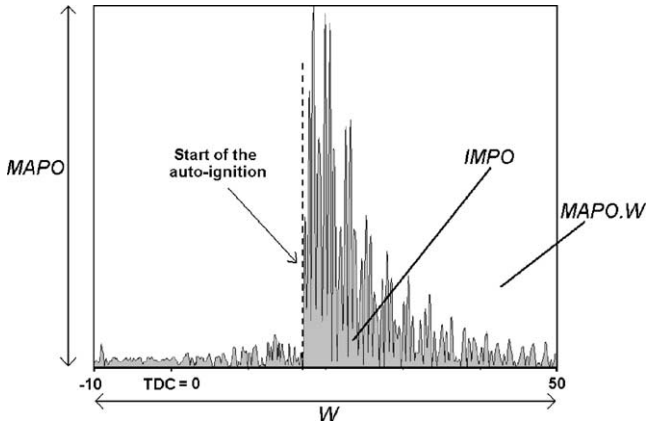

Fig. 7. *DKI* representation for a knocking cycle ($\phi = 1.0$, $\eta_v = 74\%$ and $SA = 11$ CA).

efficiency, η_v, and width of computational window, W, could have an effect on *IMPO* or *MAPO*, dimensionless analysis leads to the following expression:

$$F\big(DKI, \phi, \eta_v, (SA/W)\big) = 0 \tag{3}$$

where *DKI* is a Dimensionless Knock Indicator built from existing knock indices (*IMPO* and *MAPO*). These indices can be combined to other engine parameter in order to give an upgraded indicator. Among the different possible combinations, the following ratio is retained:

$$DKI = \frac{IMPO}{MAPO \times W} \tag{4}$$

4.1. Meaning of the DKI

A cycle by cycle analysis can be very useful to the comprehension of the *DKI* meaning. An example of high frequency pressure signal obtained in case of knocking combustion is given in Fig. 7 (where the position CA = 0 corresponds to Top Dead Center). *DKI* is the ratio between two values that can be interpreted as two surfaces. Firstly, *IMPO* is the surface under the pressure signal and secondly the quantity $MAPO \times W$ is the surface of the computational window as illustrated in Fig. 7. Consequently, the *DKI* represents the "weight" of *IMPO* within the computational window.

When the knock intensity is increased, pressure oscillations become larger. The maximum of pressure oscillations is then higher compared to the signal solely due to the normal deflagration before the auto-ignition that remains relatively constant (Fig. 8). This part of the signal can be seen as "noise" and its importance in the computational window will decrease when pressure oscillations will increase. It is then coherent to conclude that *DKI* is an "image" of the knock intensity.

DKI, defined by Eq. (4), is calculated taking into account the "noise" before the auto-ignition. In order to quantify its importance in the signal, we can remove it from the calculation by defining *IMPO*° as the integral of the signal

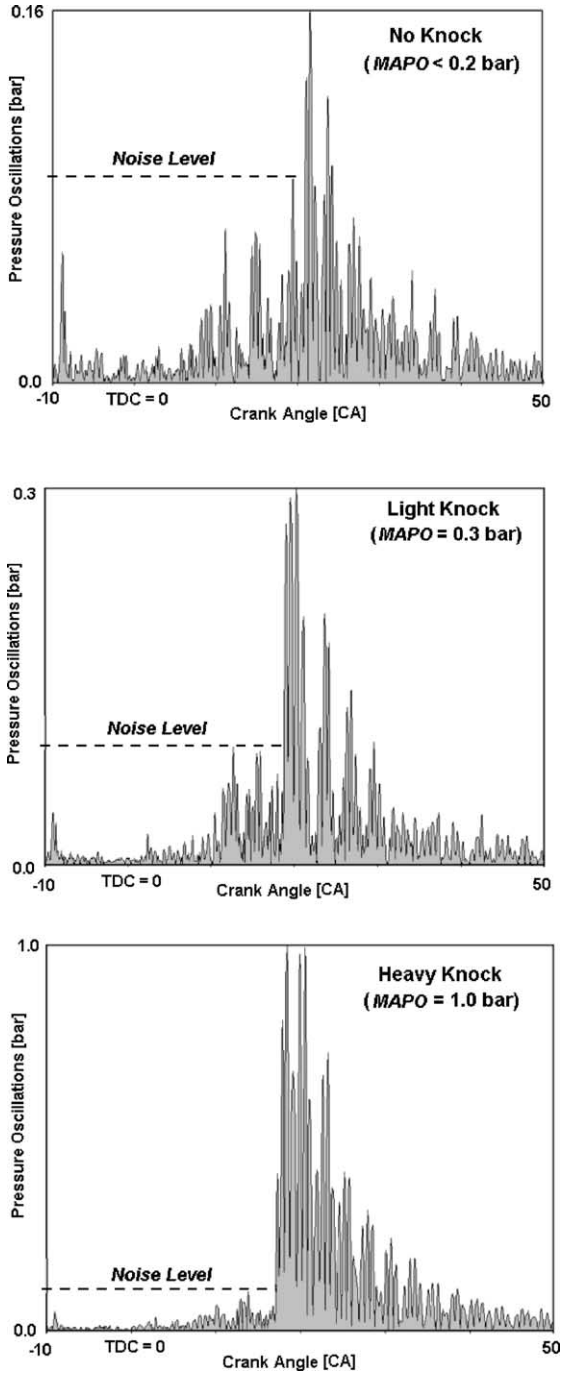

Fig. 8. *DKI* representation as a function of the knock ($\phi = 1.0$, $\eta_v = 74\%$ et $SA = 11$ CA).

starting with the auto-ignition timing. DKI° is then defined as following:

$$DKI^\circ = \frac{IMPO^\circ}{MAPO \times W} \tag{4b}$$

The results plotted in Fig. 9 show the difference between *DKI* and DKI° as a function of the knock intensity (here *MAPO*). These results confirm that the *DKI* measures the proportion of noise in the high frequency signal because $DKI - DKI^\circ$ decreases and tends to zero when knock

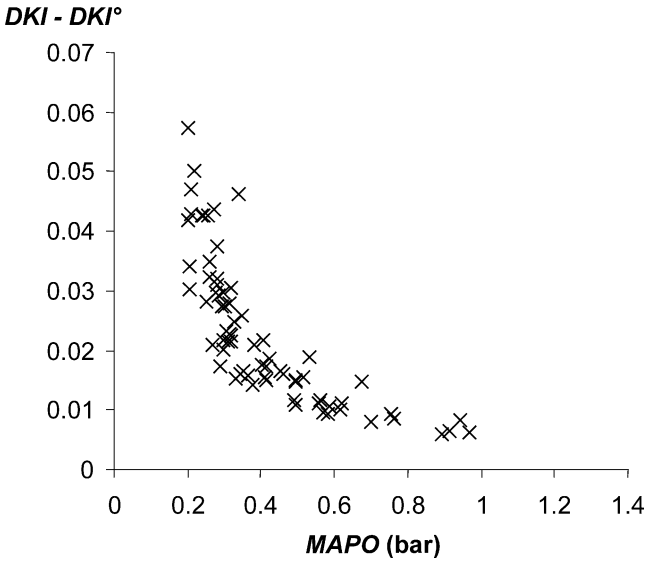

Fig. 9. Difference between *DKI* and DKI° as a function of knock intensity ($\phi = 1.0$, $\eta_v = 74\%$ and $SA = 11$ CA).

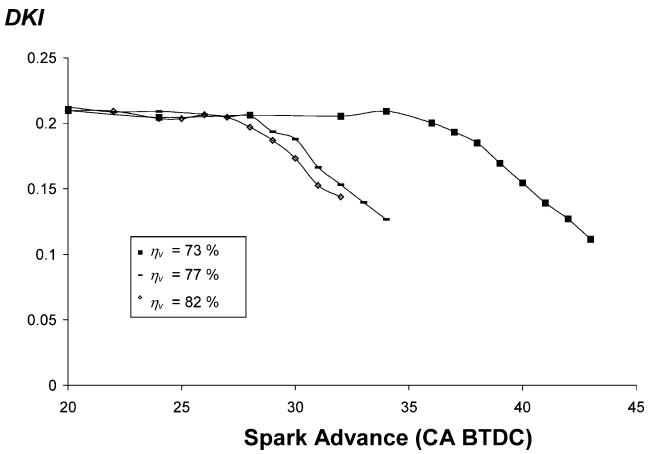

Fig. 10. *DKI* as a function of spark advance ($\phi = 0.7$).

intensity increases. Furthermore, a comprehensive analyse of experimental data show that there is no relevant effect of the engine settings on the global shape of the oscillations. Consequently, the decrease of the *DKI* is only due to the reduction of noise proportion in the computational windows. *DKI* will then decrease with the knock intensity whatever the engine geometrical characteristics and settings are.

4.2. Parametric study of the engine settings

The *DKI* studied in the following are calculated with the mean values of *IMPO* and *MAPO*. The data obtained for the three studied volumetric efficiencies are plotted in Fig. 10. It must be underlined that a constant value is obtained for spark advance preceding knock. This means that for low spark advances (without knock), the recorded signal is only composed of the "noise" from the deflagration and the *DKI* remains relatively constant. Further, its value decreases

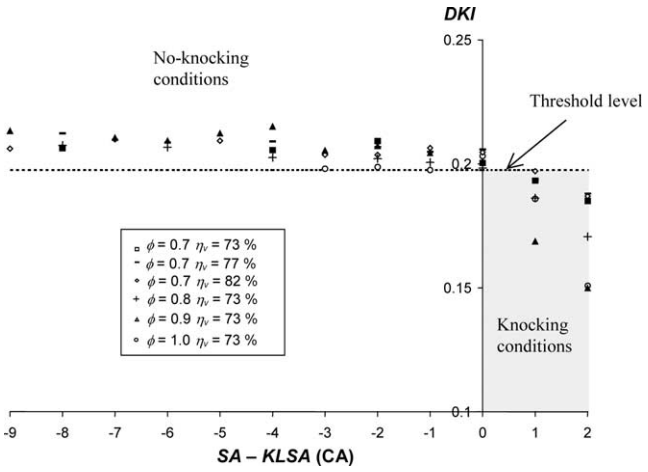

Fig. 11. Threshold level for *DKI*.

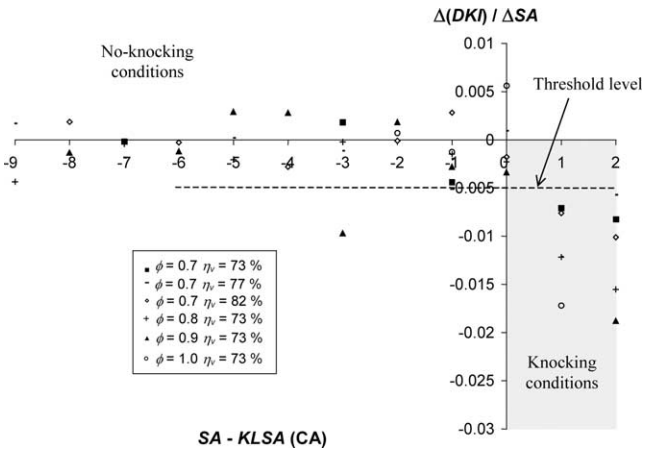

Fig. 12. Threshold level for $\Delta(DKI)/\Delta SA$.

linearly with spark advance when knock occurs because increasing the spark advance makes the knock intensity higher.

Fig. 11 presents the different results obtained when no knock occurs and for a few degrees after knock onset. In this figure, *DKI* is plotted as a function of the quantity $SA - KLSA$, quantity that we call the *KLSA* overstep. A threshold value equal to 0.197 has been set as the limit defining the *KLSA*. It is the lowest value reached by the *DKI* in the case of a normal combustion. Another possibility for the use of *DKI* consists in studying its spark advance derivative. This derivative can also be used to distinguish knocking from non-knocking conditions. Analysis of experimental data, in the same spark advance range, leads to a threshold value of the derivative equal to -5×10^{-3} CA^{-1} (Fig. 12). Rigorous identical values for *KLSA* are found by both methods.

Results acquired in knocking and non-knocking conditions are plotted in Fig. 13. An important effect of equivalence ratio on *DKI* can be seen whereas the volumetric efficiency has no significant effect. The modelling of the acquired data leads to the following correlation:

$$\frac{SA - KLSA}{W} = K\phi^a \left(\frac{IMPO}{MAPO \times W} - NL \right)^b \quad (5)$$

The values of the "noise" level *NL* (which is the mean value of the *DKI* obtained without knock) and of the coefficients K, a, b are given in Table 4. Eq. (5) was obtained with engine parameter ranges summarised in Table 5.

For the four studied equivalence ratios, the curve of Eq. (5) has been added in Fig. 13. For each *DKI* obtained, discrepancies between measured spark advance and those calculated by Eq. (5) are shown in Fig. 14. A satisfactory agreement is obtained: the *KLSA* overstep can be deduced from an *IMPO*/*MAPO* measurement with a discrepancy lower than ±0.5 CA in 75% of the cases. A discrepancy lower than ±1 CA is observed in the other 25% of the cases. These results increase the utility of the proposed indicator since it allows determining, for any engine setting, not only if knock is present but also the *KLSA* overstep. The accuracy of the method (1 CA in the worst case) is acceptable compared to other sources of uncertainty in an

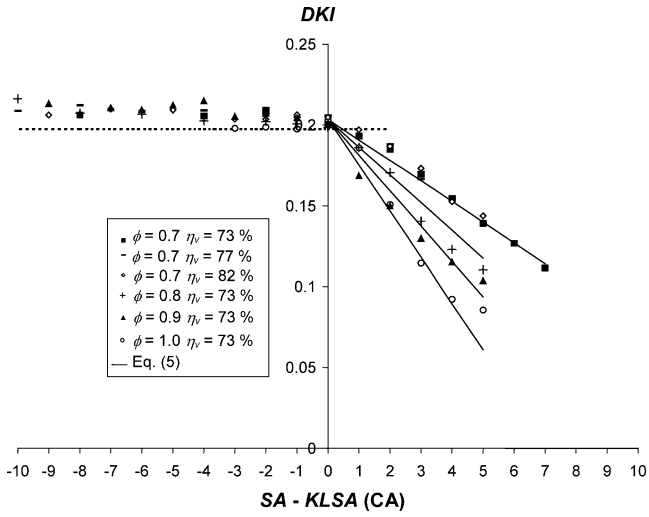

Fig. 13. Experimental and modelling results for *DKI*.

Table 4
Coefficients of Eq. (5)

NL	0.203
K	−0.60
a	−2.24
b	1

Table 5
Validity range of the modelling

	Validity range
ϕ	0.7–1.0
N	1500 rev·min^{-1}
η_v	73%–82%
$SA - KLSA$	0 CA–7 CA

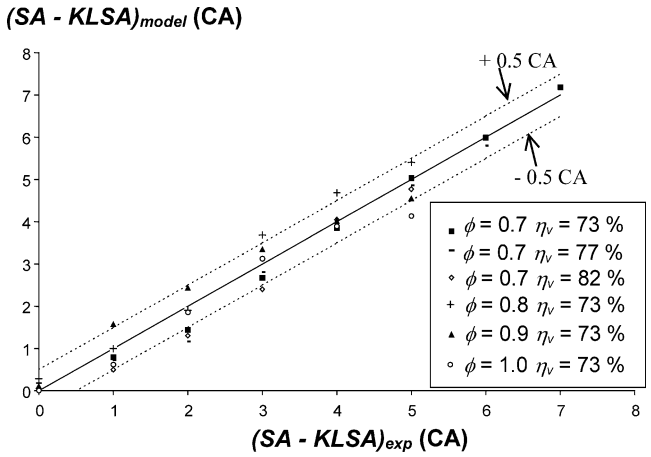

Fig. 14. Discrepancies between *KLSA* overstep measured and predicted by Eq. (5).

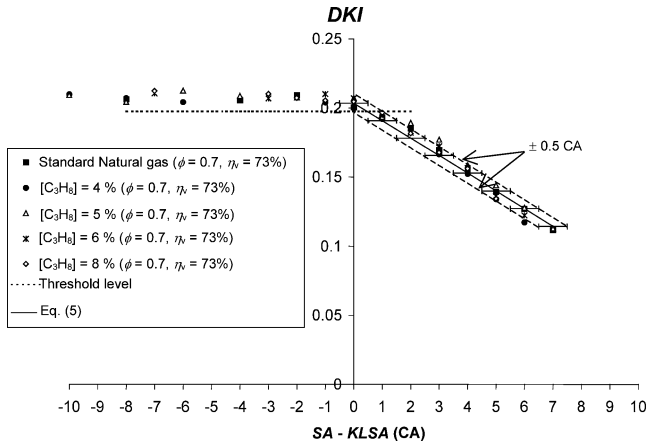

Fig. 15. *DKI* as a function of *KLSA* overstep with different propane volumetric fractions (4 to 8%).

engine operation. Moreover *KLSA* is usually determined with a 1 degree resolution such in [13,14].

As a result, a measurement of *IMPO*/*MAPO* equal to the noise level will imply an engine operation safe from knock. On the contrary, a value lower than the noise level will correspond to a knocking operation. In that case, Eq. (5) can be used to estimate the *KLSA*. Once the knock limit is known, the spark advance can be decreased down to *KLSA* − 2 CA for instance, in order to ensure free knock operation.

5. Effect of gas quality

Gas engines are subjected to variations of the natural gas quality implying changes in the non-knocking properties of the fuel. Engines, running with a constant set-up and normally operating, can suddenly be submitted to knock because of a decrease in the methane number of the fuel (due for example to an increase of heavy hydrocarbon concentration). The proposed model, Eq. (5), could be employed if it accounts for these variations. Further studies are then performed in order to quantify the effects of variations in the concentration of the components affecting significantly the methane number of the fuel. The methane number is a way to characterise the non-knocking properties of a gas [15]. It is in principle determined experimentally but it can be also calculated by a correlation from the gas composition. The Sorge et al. [16] correlation is well suited for our work. According to the synthesis work of Klimistra et al. [17], good trends are obtained by this correlation even if it may over predict the methane number. So, the Sorge et al. [16] correlation was chosen to calculate the methane numbers of the studied fuels.

The volumetric composition of the existing natural gases varies from 1 to 16% for ethane, from 0.1 to 2.5% for propane and 0 to 1% for butane [17]. This leads to a variation of the methane number for these fuels comprised between 70 and 99. In order to simulate such variations, propane is added from cylinders to the natural gas supplied by network. The concentration of propane in the fuel is increased until reaching the methane number of the poorest natural gases. Mass flow regulators maintain a constant concentration during the experiments. Equivalence ratio and volumetric efficiency are respectively set to 0.7 and 73% in the following tests. The methane number decreases when C_3H_8 concentration is increased and reaches a low enough value (68) with a propane volumetric concentration of 8% (Table 6). Results concerning effect of propane adjunction are plotted in Fig. 15. The value of *KLSA* changes with the concentration of propane (Table 6). However, it is very interesting to note that the value of *DKI* is not significantly changed with the gas quality. It is also important to underline that the threshold level of *DKI* is not modified for *KLSA* detection. In knocking conditions, Eq. (5) can predict the measured *KLSA* overstep whatever the propane concentration is. Small discrepancies are observed between predictions and measurements (less than 0.5 CA in 85% of the cases and less than 1 CA in the rest of the cases).

Table 6
Methane number and *KLSA* for the different propane concentrations

Propane volumetric fraction (%)	Methane number	*KLSA* (CA BTDC)
≈ 2 (standard natural gas)	81	36
4	76	34
5	74	34
6	72	33
8	68	33

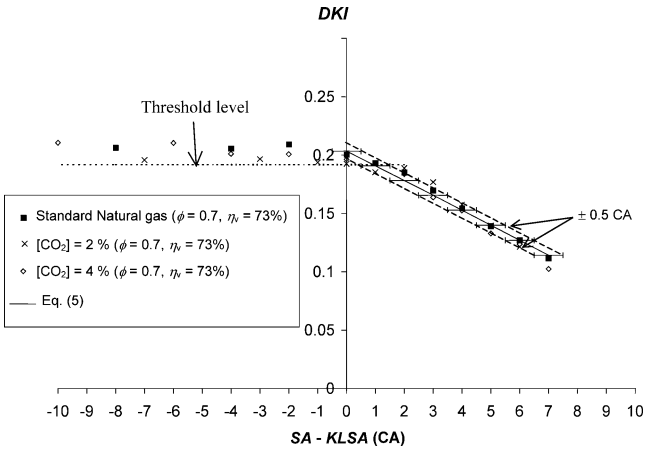

Fig. 16. *DKI* as a function of *KLSA* overstep with different carbon dioxide volumetric fractions (2 to 4%).

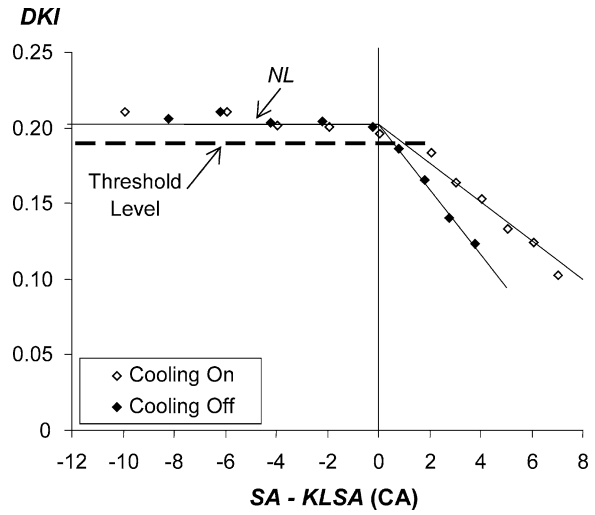

Fig. 17. *DKI* as a function of the *KLSA* overstep with and without forced air circulation intensity ($\phi = 0.7$, $\eta_v = 74\%$).

The effect of carbon dioxide concentration in the fuel is a subject of much interest too. CO_2 adjunction increases the anti-knock properties of the fuel as, for example, methanol adjunction in the case of gasoline engine [18]. *KLSA* is then increased with the CO_2 concentration. Moreover, carbon dioxide is present with the fuel when biogas, produced from fermentation of organic wastes, or by-products of gasification are burned [19]. The development of such environmentally efficient processes is important nowadays. These aspects make the study of effect of CO_2 addition essential. Experiments are conducted for CO_2 volumetric concentration of 2 and 4% in the gas. Results are plotted in Fig. 16. The values of *KLSA* and methane number are shown in Table 7 (the change of the *KLSA* value for the standard gas test compared to the value indicated in Table 6 value can be explained by the effect of ambient temperature variation as explained in details in [20]). As for the study with propane, no significant effect is observed for the indicator (Fig. 16). However, the threshold level observed for the *KLSA* determination by the *DKI* is slightly lower than in the previous cases (0.192 against 0.197) but threshold level for the derivative of the *DKI* is unchanged (-5×10^{-3} CA^{-1}). Finally, Eq. (5) can predict a *KLSA* overstep with the same accuracy as in the previous cases (less than 0.5 CA in 70% of the cases and lower than 1 CA in all other cases).

6. Generalization of the *DKI*

Because of its meaning, the *DKI* will always decrease with the knock intensity. One further test is then performed in order to check this property. The thermodynamic conditions of the combustion are changed by stopping the cooling system of our engine (previously cooled by forced air circulation). The *KLSA* measured is then very significantly decreased (by 21 CA degrees). The *DKI* measured are compared to those previously recorded in Fig. 17 for the case of a lean burn conditions. The results confirm the existence of a unique threshold level allowing to distinguish normal combustion from knock. Then, as expected, the *DKI* value decreases with the increase of knock intensity. The slope of the straight line that models this decrease depends on the engine characteristics. However, obtaining a new correlation, similar to Eq. (5) but adapted to another engine, is possible. In this new correlation, only the coefficient K, a, b and *NL* will be adjusted (they may depend on the shape and the geometry of the cylinder). This adjustment will requires only a few tests (around eight per studied equivalence ratios: three with a normal operation and five in knocking conditions).

7. Conclusion

A knock indicator based on high frequency pressure analysis was computed and analysed for a single-cylinder SI gas engine. Effects of spark advance, volumetric efficiency and equivalence ratio were studied. Adjunction of two different gases (propane and carbon dioxide) into the standard natural gas was performed. Analysis of the results led to a new dimensionless indicator: $IMPO/(MAPO \times W)$. Its use

Table 7
Methane number and *KLSA* for the different carbon dioxide concentrations

Carbon dioxide (%)	Methane number	*KLSA* (CA BTDC)
≈ 0 (standard natural gas)	80	37
2	81	39
4	83	42

enables to detect the start of knock and then to determine the *KLSA*. A relation, based on a dimensional analysis, was developed. It allows calculating the *KLSA* overstep with an uncertainty lower than 1 CA.

The *DKI* represents a valuable tool that we recommend for knock detection. Its main advantages are:

- it leads to a physically meaningful indicator that could be extended to other engines analyses,
- it gives a constant threshold level independent of the engine tunings,
- it is then easier to calibrate than *MAPO* or *IMPO* alone,
- in knocking conditions, a correlation enables to estimate the value of the *KLSA* overstep and to adequately adjust the spark advance in order to avoid knock,
- even if its computation is a slightly more complex than the one of *MAPO*, the increasing power of current computers already allows its online calculation.

Further work has now to be performed in order to extend the application field of the proposed Dimensionless Knock Indicator. The influence of engine characteristics (such as bore, compression ratio, engine speed) could be investigated in parallel with several computational parameters (such as the width of the computational window or the pass-band of pressure filtering).

References

[1] C. Mobley, Non-intrusive in-cylinder pressure measurement of internal combustion engines, SAE Paper, No 1999-01-0544 (1999).
[2] A. Auzins, H. Johansson, J. Nytomt, Ion-gap sense in misfire detection, knock and engine control, SAE Paper, No 950004 (1995).
[3] M.D. Checkel, J.D. Dale, Computerized knock detection from engine pressure records, SAE Paper, No 860028 (1986).
[4] G.T. Kalghati, M. Golombok, P. Snowdon, Fuel effects on knock, heat release and “CARS” temperatures in a spark ignition engine, Combust. Sci. Technol. 110–111 (1995) 209–228.
[5] P.V. Puzinauskas, Examination of methods used to characterize engine knock, SAE Paper, No 920808 (1992).
[6] F. Millo, C.V. Ferraro, Knock in SI engines: A comparison between different techniques for detection and control, SAE Paper, No 982477 (1998).
[7] S. Diana, V. Gilio, B. Iorio, G. Police, Evaluation of the effect of EGR on engine knock, SAE Paper, No 982479 (1998).
[8] G. Zhou, G.A. Karim, An analytical examination of various criteria for defining autoignition within heated methane–air homogeneous mixtures, Trans. ASME J. Energy Res. Technol. 116 (1994) 175–180.
[9] P.M. Najt, Evaluating threshold knock with a semi-empirical model—Initial results, SAE Paper, No 872149 (1987).
[10] M. Abu-Qudais, Exhaust gas temperature for knock detection and control in spark ignition engine, Energy Convers. Mgmt. 37 (1996) 1383–1392.
[11] J.R. Thomas, D.P. Clarke, J.M. Collins, T. Sakonji, K. Ikeda, F. Shoji, K. Furushima, A test to evaluate the influences of natural gas composition and knock intensity, Trans. ASME J. ICE 22 (1994).
[12] S. Goto, Y. Itoh, Development of lean burn high-output spark-ignited gas engines (experimental study in lean gas engines), Nippon Kikai Gakkai Ronbunshu, Trans. Japan Soc. Mech. Engrg. Part B 63 (1997) 1055–1061 (in Japanese).
[13] S. Ho, D. Amlee, R. Johns, A comprehensive knock model for application in gas engines, SAE Paper, No 961938 (1996).
[14] S. Russ, A review of the effect of engine operating conditions on borderline knock, SAE Paper, No 960497 (1996).
[15] M. Leiker, K. Christoph, M. Rankl, W. Cartellieri, U. Pfeifer, Evaluation of antiknocking property of gaseous fuels by means of methane number and its practical application to gas engines, ASME Paper, No 72-DGP-4 (1972).
[16] G.W. Sorge, R.J. Kakuezki, J.E. Peffer, Method of determining knock resistance rating for non-commercial grade natural gas, US Patent (2000) Number 6061.
[17] J. Klimstra, A.B. Hernaez, W.H. Bouwman, A. Gerard, B. Karll, V. Quinto, G.R. Roberts, H.J. Schollmeyer, Classification methods for the knock resistance of gaseous fuel—An attempt towards unification, in: Proceedings of the ICE Fall Technical Conference, Vol. 33-1, ASME, 1999, pp. 127–137.
[18] E. Moses, A.L. Yarin, P. Bar-Yoseph, On knocking prediction in spark ignition engines, Combustion and Flame 101 (1995) 239–261.
[19] S.O. Bade Shrestha, G.A. Karim, Predicting the effects of the presence of diluents with methane on spark ignition engine performance, Appl. Thermal Engrg. 21 (2001) 331–342.
[20] G. Brecq, J. Bellettre, M. Tazerout, T. Muller, Knock prevention of gas SI engine by adjunction of inert gases to the fuel, in: Proceedings of the International Joint Power Generation Conference, ASME, 2002 (8p. on CDROM).